

TKN: Transformer-based Keypoint Prediction Network For Real-time Video Prediction

HAORAN LI, University of Science and Technology of China, China

XIAOLU LI, University of Science and Technology of China, China

YIHANG LIN, University of Science and Technology of China, China

YANBIN HAO, University of Science and Technology of China, China

HAIYONG XIE, Adv. Innovation Center for Human Brain Protection, Capital Medical University, China

PENGYUAN ZHOU, Aarhus University, Denmark

YONG LIAO*, University of Science and Technology of China, China

Video prediction is a complex time-series forecasting task with great potential in many use cases. However, conventional methods overemphasize accuracy while ignoring the slow prediction speed caused by complicated model structures that learn too much redundant information with excessive GPU memory consumption. Furthermore, conventional methods mostly predict frames sequentially (frame-by-frame) and thus are hard to accelerate. Consequently, valuable use cases such as real-time danger prediction and warning cannot achieve fast enough inference speed to be applicable in reality. Therefore, we propose a transformer-based keypoint prediction neural network (TKN), an unsupervised learning method that boost the prediction process via constrained information extraction and parallel prediction scheme. TKN is the first real-time video prediction solution to our best knowledge, while significantly reducing computation costs and maintaining other performance. Extensive experiments on KTH and Human3.6 datasets demonstrate that TKN predicts 11 times faster than existing methods while reducing memory consumption by 17.4% and achieving state-of-the-art prediction performance on average.

CCS Concepts: • **Do Not Use This Code** → **Generate the Correct Terms for Your Paper**; *Generate the Correct Terms for Your Paper*; Generate the Correct Terms for Your Paper; Generate the Correct Terms for Your Paper.

Additional Key Words and Phrases: Video prediction, real-time, keypoint, transformer.

ACM Reference Format:

Haoran Li, Xiaolu Li, Yihang Lin, Yanbin Hao, Haiyong Xie, Pengyuan Zhou, and Yong Liao. 2018. TKN: Transformer-based Keypoint Prediction Network For Real-time Video Prediction. *J. ACM* 37, 4, Article 111 (August 2018), 20 pages. <https://doi.org/XXXXXXXX.XXXXXXX>

1 INTRODUCTION

Predicting the future has always been a coveted ability that allows users to be well prepared for upcoming events. With the advancement of artificial intelligence in the field of computer vision,

Authors' addresses: Haoran Li, lhr123@mail.ustc.edu.cn, University of Science and Technology of China, Hefei, China; Xiaolu Li, xiaoluli0718@mail.ustc.edu.cn, University of Science and Technology of China, Hefei, China; Yihang Lin, lyh1998@mail.ustc.edu.cn, University of Science and Technology of China, Hefei, China; Yanbin Hao, haoyanbin@hotmail.com, University of Science and Technology of China, Hefei, China; Haiyong Xie, haiyong.xie@ieee.org, Adv. Innovation Center for Human Brain Protection, Capital Medical University, Beijing, China; Pengyuan Zhou, pengyuan.zhou@ece.au.dk, Aarhus University, Aarhus, Denmark; Yong Liao, yliao@ustc.edu.cn, University of Science and Technology of China, Hefei, China.

Permission to make digital or hard copies of all or part of this work for personal or classroom use is granted without fee provided that copies are not made or distributed for profit or commercial advantage and that copies bear this notice and the full citation on the first page. Copyrights for components of this work owned by others than ACM must be honored. Abstracting with credit is permitted. To copy otherwise, or republish, to post on servers or to redistribute to lists, requires prior specific permission and/or a fee. Request permissions from permissions@acm.org.

© 2018 Association for Computing Machinery.

0004-5411/2018/8-ART111 \$15.00

<https://doi.org/XXXXXXXX.XXXXXXX>

the ability to predict the future is gradually becoming a reality. One of the most popular methods is video prediction, which predicts subsequent video frame sequences based on prior ones. It belongs to the time series prediction problem and was initially applied to the prediction of radar echo maps of precipitation [26] then to human activities [31, 32]. Current mainstream video prediction methods can be divided into two categories. The first is to improve the well-known recurrent neural network (RNN) to accurately capture the inter-frame pattern [31, 32, 34]. However, RNN-based methods often gradually lose the initial information during the sequential information transmission across the hidden layers, resulting in the so-called *short memory* that negatively impacts the long sequence prediction accuracy [37]. The second category divides a video frame into a moving portion and a stationary portion and then predicts the two portions separately [10, 11, 21, 36].

Most existing works focus on improving accuracy by a few percentage points while ignoring the prediction speed, which is actually crucial for many real-time applications. For instance, in a speeding car, the driver can typically afford a reaction time to danger below 3 seconds [19] otherwise would face a grave risk. Assume we want to predict the video frames for the next 3 seconds with a typical vehicular front camera rate of 60 frames per second (fps), the video prediction method has to reach at least 180fps to finish the prediction within one second. However, existing methods can normally support a frame rate only up to 80 to 100 fps [1, 10, 11], which can barely help in reality. The reason is threefold: 1) existing methods extract complex features for the sake of higher accuracy, resulting in an excessive number of floating point operations [1, 5, 31]; 2) they waste considerable time on learning similar background information often shared by consecutive frames [13, 25]; 3) they use a sequential prediction process where the next frame's input depends on the previous frame's output. Consequently, these methods are poor at processing efficiency and can not predict multiple frames in parallel.

As such, we propose a Transformer-based Keypoint extraction neural Network (TKN), which is an unsupervised learning method consisting of a keypoint detector and predictor. TKN can predict video frames by predicting only the keypoints. The keypoint detector extracts feature data for only a few tens of bytes and achieves temporal parallelism, hence greatly reducing the number of floating-point operations, the prediction time, and memory consumption. The predictor further accelerates the process by gathering global attention information in a parallel manner via a self-attention mechanism without disregarding past information. Our contributions are threefold as follows.

- TKN incorporates the advantages of both Keypoint and Transformer structures to guarantee high prediction accuracy, fast training and testing, and low memory consumption. In order to accurately predict videos that contain frequent changes, we additionally propose a sequential variation of TKN called TKN-Sequential.
- The keypoint detector of TKN predict multiple frames in parallel and outperforms keypoint-based state-of-the-art (SOTA) methods in the field of video prediction in terms of keypoint capture and frame reconstruction, resulting in increasing SSIM by 6.3% and PSNR by 7.5% with 88.1% fewer floating-point operations.
- Extensive experimental evaluations have demonstrated the superiority of TKN which achieves a prediction speed of 1176 fps and thus realizing the first real-time video prediction to our best knowledge. Compared to existing methods, TKN is 11 times faster at prediction while reducing 17.4% GPU memory consumption. As such, TKN lays the groundwork for future real-time multimedia technologies.

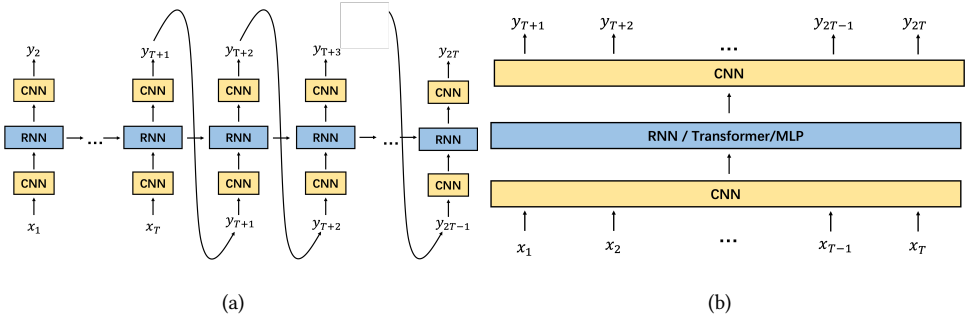


Fig. 1. (a) The sequential prediction scheme generally takes a long time to predict frames due to the sequential scheme. (b) The parallel prediction scheme we propose can greatly accelerate the prediction speed.

2 RELATED WORKS

Unsupervised methods can reduce the cost of manual annotation which is a common requirement for video datasets.

Unsupervised keypoint learning. Due to the similarity of pixels in consecutive video frames, the keypoints in each frame can be learned via unsupervised reconstruction of the other frames. Jakob *et al.* [14] propose to learn the object landmarks via conditional image generation and representation space shaping. Minderer *et al.* [21] introduce keypoints to video prediction using stochastic dynamics learning for the first time, which drastically reduces computational complexity. Gao *et al.* [10] applied grids on top of [21] for a clearer expression of the keypoint distribution.

Unsupervised video prediction uses the pixel values of the video frames as the labels for unsupervised prediction. Existing studies can be classified into two categories, as shown by Fig. 1(a). The first category of works focuses on improving the performance of the well-known RNN by adapting the intermediate recurrent structure [4, 22, 30, 31, 34]. For example, E3D-LSTM [31] integrates 3DCNN with LSTM to extract short-term dependent representations and motion features. PredRNN [34] enables the cross-level communication for the learned visual dynamics by propagating the memory flow in both bottom-up and top-down orientations. The second category focuses on disentangling the dynamic objects and the static background in the video frames, mostly by adapting the CNN structure [3, 7, 11, 35, 36]. For instance, DGGAN [36] trains a multi-stage generative network for prediction guided by synthetic inter-frame difference. PhyDNet [11] uses a latent space to untangle physical dynamics from residual information.

The methods in both categories use so-called “sequential prediction”, that is, using the previous prediction frame as the input frame for the next round of prediction. The prediction speed is proportional to the number of frames to be predicted and thus leads to an intolerably long delay for long-term prediction. Therefore, we propose a parallel prediction scheme, as shown in Fig. 1(b), to extract the features of multiple frames and output multiple predicted frames in parallel, which greatly accelerates the prediction process.

Transformer has been utilized extensively in NLP due to its benefits over RNN in feature extraction and long-range feature capture. It monitors global attention to prevent the loss of prior knowledge which often occurs with RNN. Its parallel processing capacity can significantly accelerate the process. Recently, the field of computer vision has begun to explore its potential and produced positive results [2, 8, 15–17]. Most related works input segmented patches of images to the transformer to calculate inter-patch attention and obtain the features. There are also a number of vision transformer

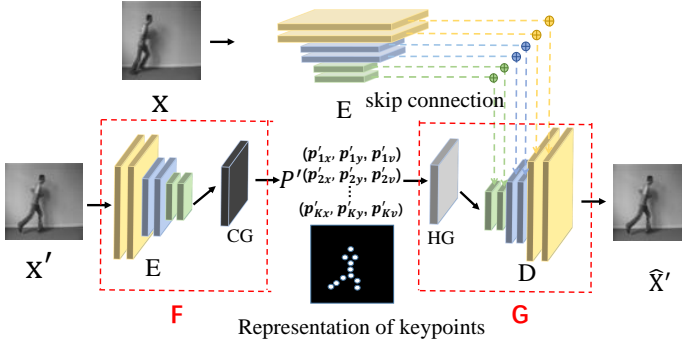


Fig. 2. Detailed structure of Keypoint Detector

(VIT) approaches applied to video analysis. For example, VIVIT [2] proposes four different video transformer structures to solve video classification problems using the spatio-temporal attention mechanism. [18] applies the swin transformer structure to video and uses an inductive bias of locality. In this paper we select CNN as the feature extractor instead of the VIT structure because of the huge computational cost of VIT compared to CNN. We select the transformer structure as the predictor because it outperformed RNN, mix-mlp, and other structures, in terms of predicting spatio-temporal features in our empirical experiments.

Most of the aforementioned video prediction methods extract from each frame complex features, typically of tens of thousands of bytes [1, 11, 26, 31], resulting in excessive numbers of floating point operations in both the feature extraction module and the prediction module. Moreover, they employ sequential (frame-by-frame) prediction process. Hence, both training and testing consume a great deal of time and memory. In the meanwhile, many videos, particularly human activity records, have a significant amount of background redundancy [13, 25] that can be removed by extracting information only from the key motions. Therefore, in this work, we try to couple the unique advantages of the transformer and the keypoint-based prediction methods to maximize their benefits.

3 MODEL

We start by formally defining the video prediction problem as follows. Given a stream of n continuous video frames, $X = (X_{t-n+1}, \dots, X_{t-1}, X_t)$, $X_i \in \mathbb{R}^{H \times W \times C}$ denotes the i -th frame for which H , W , and C denote the height, width, and number of channels, respectively. The objective is to predict the next m video frames $Y = (Y_{t+1}, Y_{t+2}, \dots, Y_{t+m})$ using the input X .

$$(X_{t-n+1}, \dots, X_{t-1}, X_t) \xrightarrow{\text{predict}} (Y_{t+1}, Y_{t+2}, \dots, Y_{t+m}). \quad (1)$$

Next, we present the dedicated design of TKN for this task. As depicted in Figure 4, TKN consists of two main modules, namely, the keypoint detector and the predictor module.

3.1 Keypoint Detector

TKN employs a keypoint detector to detect the keypoints that are most likely moving. As illustrated in Figure 2, the detector extracts the keypoints as coordinate points. Here we describe the abstract

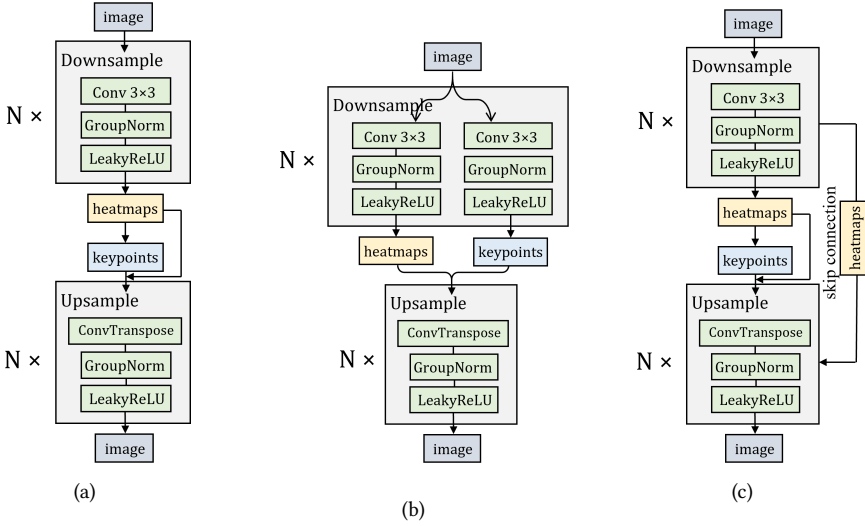


Fig. 3. Comparison of three different encoder and decoder structures. (a) The structure proposed by [21] requires more network layers while performing poorly at disentangling keypoints and background information. (b) A structure that can well disentangle keypoints and background information at the cost of complex network architecture and high computation cost. (c) We adopt the well-known skip connection to achieve good performance on information disentangling with simple structure.

representation, training procedure, and the structures of the encoder and the decoder. Please refer to the supplemental material for additional information.

Abstract representation. Let $X, X' \in X$ denote any two frames in X , and X referred as the source frame and X' the target frame. The keypoints in a video frame can be represented by $P = (p_1, p_2, \dots, p_K) \in \Omega^K$, where K represents the number of keypoints, Ω the coordinates. Assume that function \mathbb{F} can extract the keypoints and \mathbb{G} can reconstruct the target frame X' by using K keypoints of X' and the features of the source frame X :

$$\begin{cases} \mathbb{F}(X') = P' \\ \mathbb{G}(X; P') = \hat{X}' \end{cases} \quad (2a) \quad (2b)$$

where \hat{X}' denotes the reconstructed frame. By minimizing the difference between \hat{X}' and X' , the P' obtained by \mathbb{F} represents the different parts between X and X' , which become what we call *keypoints*. We use the pixel-wise L_2 frame loss to measure the difference between X' and \hat{X}' as follows:

$$L_{rec} = \|X' - \hat{X}'\|_2. \quad (3)$$

\mathbb{F} and \mathbb{G} can be learned using L_{rec} in an end-to-end unsupervised learning process without labeling X or X' .

As shown in Figure 2, \mathbb{F} consists of a n -layer CNN encoder E , and a coordinate generator CG which converts each heatmap output of E to $p'_i = (p'_{ix}, p'_{iy}, p'_{iv})$, where p'_i denotes the i -th keypoint of X' , (p'_{ix}, p'_{iy}) represents the coordinates of p'_i and p'_{iv} denotes the intensity. \mathbb{G} consists of a heatmap generator HG which converts the K keypoints to a heatmap and a n -layer CNN decoder D which has a symmetrical structure with E .

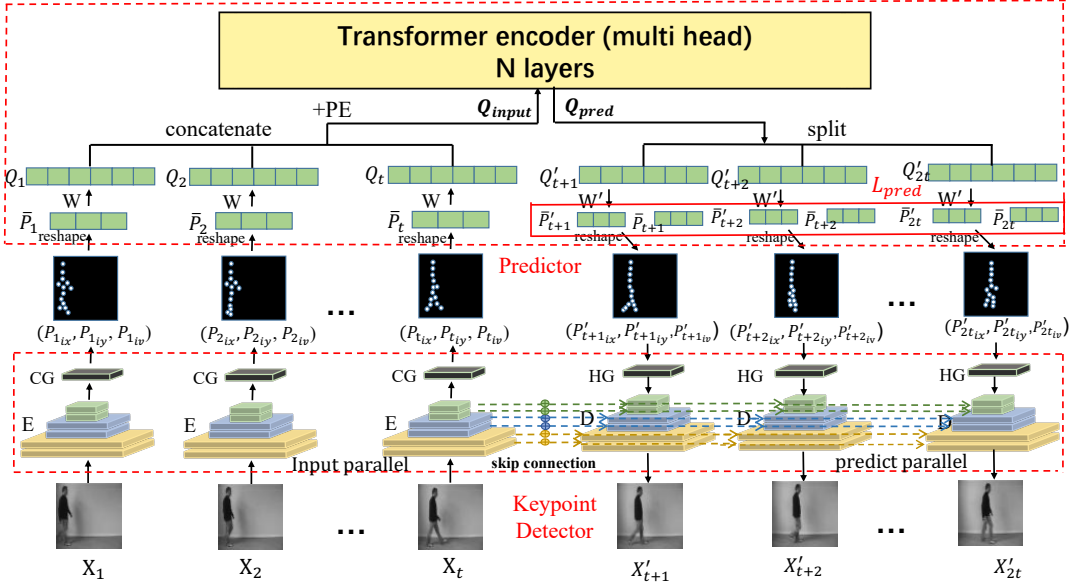


Fig. 4. Detailed structure of TKN. Two main modules are the Keypoint Detector and the Predictor marked with the red dashed lines. The predicted frame uses the background information extracted from the last frame of the input. Both the inputting stage and prediction stage allow batch processing (e.g., input multiple frames simultaneously) and thus enable temporal parallelism. Note that the ground truth keypoints information, $P_{real} = (\bar{P}_{t+1}, \dots, \bar{P}_{2t})$, is output by X_{t+1}, \dots, X_{2t} using keypoint detector (excluded from the figure for simplicity).

Encoder and Decoder. We compared three structures of the encoder and the decoder. The first structure, as shown in Fig. 3(a), is proposed by Minderer *et al.* [21], in which the output heatmaps serves both as the generation feature of keypoints and the input feature for the background of the decoder (the heatmaps here corresponds to X in Eq. (2b)). Although this structure is simple, it needs a lot of encoder layers and a high feature dimension to extract both key points and background information. Besides, our experimental results show that this structure does not perform well in reconstructing the target frame. The structure in Fig. 3(b) uses two networks to extract the keypoints information and the background information separately. While it performs well at information disentangling in our experiments, its structure is too complex and thus requires high computation cost. Therefore, in TKN we design a structure shown in Fig. 3(c) adopting the “skip connection” proposed by [24], to allow the encoder to disentangle the background information layer by layer and only focus on outputting the keypoints, and synthesize the disentangled background information into the decoder via skip connection. Experimental results show that the structure in Fig. 3(c) can reconstruct frames better with a lower computation cost.

Let E_i denote the i -th layer of E and $h_i \in \mathbb{R}^{H_i \times W_i \times C_i}$ denote its output heatmap, where $h'_1 = E_1(X')$ and each subsequent layer can be expressed as follows:

$$E_i(h'_{i-1}) = h'_i, i \in \{2, n\}. \quad (4)$$

The output of the last layer h'_n is fed into coordinate generator CG to extract the keypoints :

$$CG(h'_n) = (p'_1, \dots, p'_i, \dots, p'_K). \quad (5)$$

Coordinate Generation (CG) module converts the heatmap generated by the encoder's last layer to the keypoints. We use a similar CG structure as in [14] which first uses a fully connected layer to convert the encoder heatmap h_n from $\mathbb{R}^{H_n \times W_n \times C_n}$ into $\mathbb{R}^{H_n \times W_n \times K}$, where K refers to the number of keypoints. We do this in the hope of compressing $H_n \times W_n$ into the form of point coordinates in the dimension of K . The converted heatmap h'_n can be rewritten as $h'(x; y; i)$, where $x = 1, 2, \dots, W_n, y = 1, 2, \dots, H_n, i = 1, 2, \dots, K$, represent the three dimensions of h'_n , respectively. Then we can calculate the coordinates of the k -th keypoint in width p_{ix} as follows:

$$h'_n(x; i) = \frac{\sum_y h'_n(x; y; i)}{\sum_{x,y} h'_n(x; y; i)}, \quad (6)$$

$$p_{ix} = \sum_x h_x h'_n(x; i), \quad (7)$$

where h_x is a vector of length W_n consisting of values uniformly sampled from -1 to 1 (for example, if $W_n = 4$ then $h_x = [-1, -0.333, 0.333, 1]$). By doing so, we add an axis to the heatmaps at the dimension W_n where p_{ix} is the position of the i -th keypoints on the width. Similarly, we can calculate the coordinate in height p_{iy} by exchanging the position of x and y using Equation (6) and Equation (7). We also need the feature values at these coordinates to reconstruct the following frames with keypoints. We express such values with the averages on both the H_n and W_n dimension. We use p_{iv} to represent the value of the k -th keypoint:

$$p_{iv} = \frac{1}{H_n \times W_n} \sum_{x,y} h_n(x; y; i). \quad (8)$$

As such, we extract the keypoints as $p_i = (p_{ix}, p_{iy}, p_{iv}), i = 1, 2, \dots, K$.

Next, the features of X and P' are input to \mathbb{G} as shown in Eq. (2b). The features of $X, h_n \in \mathbb{R}^{H_n \times W_n \times C_n}$, are obtained via E . P' is converted to a heatmap h'_p via HG :

$$HG(p'_1, \dots, p'_i, \dots, p'_K) = h'_p. \quad (9)$$

Heatmap Generation (HG) module is a reversed process of CG that converts coordinates to the heatmap. We use a 2-D Gaussian distribution to reconstruct the heatmaps. We first convert the coordinates p_x, p_y into 1-D Gaussian vectors, x_{vec} and y_{vec} , where $p_x = (p_{1x}, p_{2x}, \dots, p_{Kx}), p_y = (p_{1y}, p_{2y}, \dots, p_{Ky})$, as follows:

$$x_{vec} = \exp\left(-\frac{1}{2\sigma_2} \|p_x - \bar{p}_x\|^2\right), \quad (10)$$

$$y_{vec} = \exp\left(-\frac{1}{2\sigma_2} \|p_y - \bar{p}_y\|^2\right), \quad (11)$$

where \bar{p}_x and \bar{p}_y are the expectations of p_x and p_y , respectively. By multiplying x_{vec} and y_{vec} we can get the 2-D Gaussian maps G_maps as follows:

$$G_maps = x_{vec} \times y_{vec}. \quad (12)$$

Finally we calculate the Hadamard product of G_maps and p_v to get the h'_p :

$$h'_p = G_maps \circ p_v. \quad (13)$$

We align the dimension of h'_p with h_n to allow their direct concatenation sent to the decoder for reconstruction. As mentioned, inspired by the "skip connection" in UNet [24] and Ladder Net [23], which can reconstruct images better with fewer encoder and decoder layers, we input the heatmaps h_1, h_2, \dots, h_n obtained by each encoder layer to the decoder through "skip connection". Let D_i denote

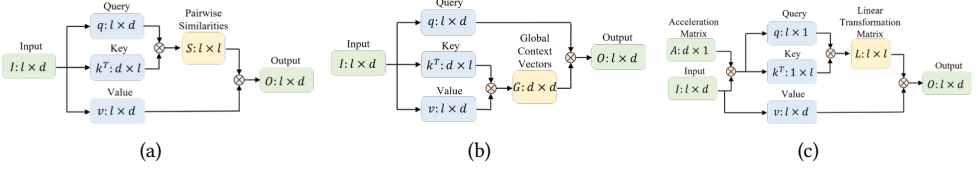


Fig. 5. Three different attention mechanism structures: (a) is the original dot-product structure, with a computational complexity of $O(l^2d)$; (b) is the linear attention structure, with a computational complexity of $O(ld^2)$; (c) is the structure we propose, which uses an acceleration matrix A to reduce the computational complexity of the linear transformation matrix L to $O(l(d + l)^2)$.

the i -th decoder layer and d_i denote its output heatmap, where $d_1 = D_1(\text{concat}(h'_p, h_n))$ and each subsequent layer can be expressed as follows:

$$d_i = D_i(\text{concat}(d_{i-1}, h_{n-i+1})), i \in \{2, n\}, \quad (14)$$

where d_n is \hat{X}' . In this manner, the decoder learns the “background” (i.e., the static information) features eliminated by the encoder, thus improving the higher level representation details of the model. The additional “background” information also allows the encoder to focus more on the keypoints.

3.2 Predictor

The original prediction task is transformed, via the keypoint detector’s encoding, into predicting the subsequent m groups of keypoints P_{t+1}, \dots, P_{t+m} , based on the prior n groups of keypoints P_{t-n+1}, \dots, P_t . We select the transformer[29] as the predictor because it can associate keypoint information at each moment through attention, making it less prone to forgetting compared to sequential networks like RNNs. We found that using only the transformer’s encoder for encoding temporal relationships between keypoints leads to better and faster predictions than using the entire structure.

Transformer uses the attention mechanism, utilizing query (q), key (k), and value (v) to compute the correlation between sequence nodes. The computational complexity of this attention is $O(l^2d)$ (l represents the sequence length, and d is the dimension of the sequence) as shown in Fig.5(a). Many methods aim to reduce attention’s computational complexity, such as linear attention, which assumes $l \gg d$ in natural language processing and results in a complexity of $O(ld^2)$ as shown in Fig.5 (b). However, in video prediction, $l < d$, so such improvements would increase computational complexity. To address this, we introduce an acceleration matrix $A \in R^{d \times 1}$, which, when multiplied with the input I , yields q_A and k_A matrices with reduced dimensions. We then compute the linear transformation matrix $L = q_A k_A^T$ to reduce the computational complexity to $O(ld + l^2)$ as shown in Fig.5 (c). This reduces the overall complexity by half. We only apply this operation to the qk^T matrix to maintain prediction accuracy.

The transformer encoder requires the input to be a one-dimensional vector with a length of $d_m \text{odel}$, e.g., (512,768,1024). Hence we first convert the K keypoint-triples $\{(p_{ix}, p_{iy}, p_{iv}) | i = 1, \dots, K\}$ to a one-dimensional vector \bar{P} :

$$\bar{P} = (p_{1x}, p_{1y}, p_{1z}, \dots, p_{Kx}, p_{Ky}, p_{Kz}) \quad (15)$$

\bar{P} represents the low-dimensional *explicit* spatial coordinates. Inputting \bar{P} directly into the transformer necessitates adjusting the dimension of the intermediate parameter values according to K in each prediction instance. Consequently, training and testing would become difficult.

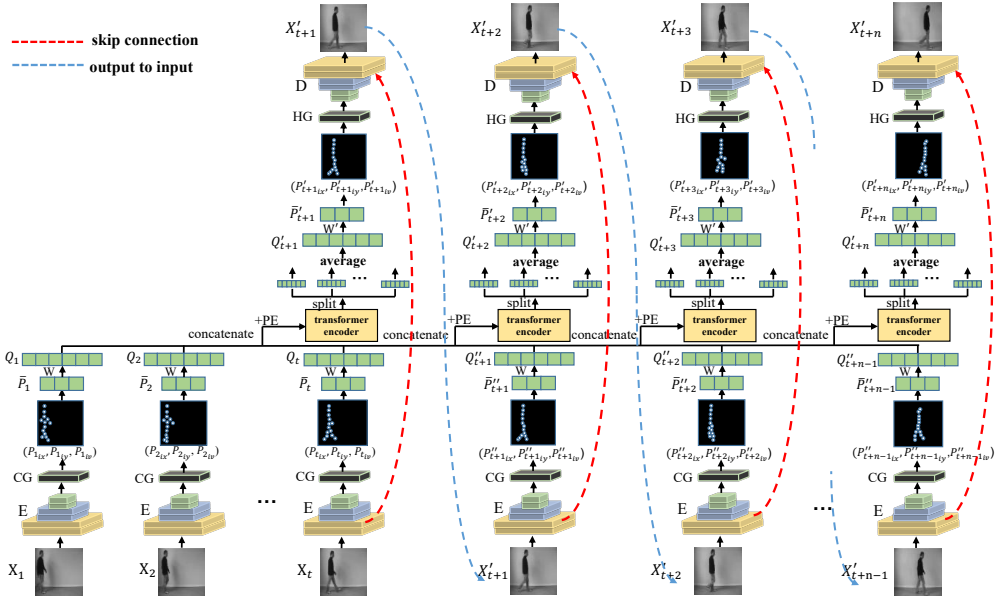


Fig. 6. Detailed structure of TKN-Sequential. It uses the same keypoint detector and predictor structures with TKN but has a different prediction process. Particularly, it uses the previous predicted frame's background as the following one's to ensure background consistency.

The predicted keypoints sequence is obtained through linear transformation of the input keypoints sequence. However, real-world object motion is often complex and better represented by differential equations. By transforming the explicit input into a higher-dimensional latent space, the keypoint sequence features can be predicted through linear transformation. Moreover, many works [20, 27, 38] have demonstrated the benefits of *latent* representations. We also found latent representations well capture the regularity of keypoints over time in our experiments. Therefore, we use a matrix to map the explicit coordinates representation to a latent space to obtain a high-dimensional latent representation vector. Specifically, we convert the variable-length and low-dimensional \bar{P} to a fixed-length and high-dimensional Q by converting \mathbb{R}^{3K} to $\mathbb{R}^{d_{model}}$ via a mapping matrix W : $Q = W \cdot \bar{P}$. where $W \in \mathbb{R}^{d_{model} \times 3K}$. To compensate the lack of time-sensitive capability, we manually add location information embedding (PE) to Q ,

$$Q_{input} = \text{concat}(Q_{t-n+1}, \dots, Q_t) + PE, \quad (16)$$

where PE is the trigonometric function as defined in [29]. The number of input sequences and output sequences are equal for the transformer encoder. Therefore, we can use transformer encoder to get the predictions Q'_{t+1}, \dots, Q'_{2t} using the input Q_{input} :

$$Q'_{t+1}, \dots, Q'_{2t} = \text{Trans_encoder}(Q_{input}). \quad (17)$$

Finally, we use an invert mapping matrix $W' \in \mathbb{R}^{3K \times d_{model}}$ to reconstruct the high-dimensional sequence $Q_{pred} = (Q'_{t+1}, \dots, Q'_{2t})$ back to the low-dimensional keypoints spatio-temporal sequence P_{pred} , which is then input to the decoder to generate the predicted frames:

$$P_{pred} = W' \cdot Q_{pred}. \quad (18)$$

We only need to calculate the loss of sequence $P_{real} = (\bar{P}_{t+1}, \dots, \bar{P}_{2t})$ which is output by X_{t+1}, \dots, X_{2t} using keypoint detector and P_{pred} to complete the training of the predictor using a well-trained keypoint detector, for which we also use the L_2 loss:

$$L_{pred} = \|P_{real} - P_{pred}\|_2. \quad (19)$$

3.3 Prediction Processes

Sequential prediction is time consuming. Since most subsequent frames in high frame-rate videos are fairly similar, we can use the background of the frame immediately just before the prediction target as the background of the prediction target frame. We can then combine the predicted keypoints with the background to generate the integrated predicted frames. As illustrated in Fig. 4, we integrate the P_{pred} generated by Transformer encoder to the background of t -th frame and directly generate the subsequent t prediction frames $X'_{t+1}, X'_{t+2}, \dots, X'_{2t}$. This parallel prediction mechanism, i.e., TKN, can input and predict multiple frames as batches to significantly accelerate the prediction process.

We reason that frame-by-frame prediction structure has higher accuracy to predict frames with frequent changes (as proved by experiment results). Hence we also provide a sequential variation of TKN, TKN-Sequential, which uses the previous predicted frame's background as the following one's to ensure background consistency. Fig. 6 shows the detailed structure of TKN-Sequential and Fig. 6 depicts its comparison with TKN.

Since the output of the transformer encoder has the same length as the input sequence, we take the averaged predictor's output as the predicted frame. Suppose we have predicted i frames, $Q'_{t+1}, \dots, Q'_{t+i}$, then Q'_{t+i+1} can be expressed as:

$$Q'_{t+i+1} = \frac{1}{t+i} \sum_{j=1}^{t+i} Trans_encoder(Q_{input}; j), \quad (20)$$

where $Q_{input} = concat(Q_{t-n+1}, \dots, Q_t, Q'_{t+1}, \dots, Q'_{t+i}) + PE$ according to (16).

X'_{t+1} is the combination of predicted \bar{P}'_{t+1} and the background information of X_t extracted by the decoder. Note that " \bar{P}'_{t+1} and the background information of X'_{t+1} " are not equal to " \bar{P}'_{t+1} and the background information of X_t ", albeit they are both extracted by the encoder from the X'_{t+1} . It is because two consecutive frames are very similar but still have some minor differences in the keypoints and background information, otherwise it would be no different from multi-frame prediction process.

4 EXPERIMENTAL SETUP

Dataset. We used two real action datasets, KTH [25] and Human3.6 [13], to verify the real-time and efficient performance of the proposal under different patterns.

- KTH dataset includes 6 types of movements (walking, jogging, running, boxing, hand waving, and hand clapping) performed by 25 people in 4 different scenarios, for a total of 2391 video samples. The database contains scale variations, clothing variations, and lighting variations. We use people 1–16 for training and 17–25 for testing. Each image is converted to the shape of (64, 64, 3).
- Human3.6 dataset contains 3.6 million 3D human poses performed by 11 professional actors in 17 scenarios (discussion, smoking, taking photos and so on). We use scenario 1, 5, 6, 7, and 8 for training and 9 and 11 for testing. Each image is converted to the shape of (128, 128, 3).

Implementation. The experiments were run on a server equipped with an Nvidia GeForce RTX 3090 GPU. We conducted a two-step training: first we trained the keypoint detector using L_{rec} in

Dataset	Method	SSIM \uparrow	PSNR \uparrow	TIME (s) \downarrow (train)	TIME (ms) \downarrow (test)	FPS \uparrow (test)	Memory (MB) \downarrow (train)	Memory (MB) \downarrow (test)
KTH	ConvLSTM	0.712*	23.58*	61	72	278	8,055	1,779
	PredRNN	0.839*	27.55*	204	184	109	6,477	1,721
	PredRNNv2	0.838*	28.37*	246	222	90	8,307	1,779
	PhyDNet	0.854	26.9	108	240	83	8,491	2,704
	SLAMP	0.864*(30)	28.72(30)	465	388	52	21,103(16)	2,295
	E3D-LSTM	0.879*	29.31*	879	338	59	21,723(16)	2,687
	Grid-Keypoint	0.837*	27.11*	145	252	79	12,661	2,259
	Struct-VRNN	0.766*	24.29*	111	151	132	5,661	1,817
	TKN (w/o tp)	0.871	27.71	35	86	233	3,777	1,447
	TKN-Sequential	0.862	27.73	44	154	130	6,309	1,785
TKN	0.871	27.71	35	17	1,176	4,945	1,705	
Human3.6	ConvLSTM	0.776*	-	63	32	125	6,561	1,857
	PredRNN	0.781*	-	462	47	85	5,829	1,743
	E3D-LSTM	0.869*	-	3154	167	24	18,819(8)	5,767
	PhyDNet	0.901*	-	207	88	45	12,213	2,353
	Grid-Keypoint	0.928	28.76	114	106	38	9,891	2,003
	Struct-VRNN	0.916	26.97	67	41	98	5,015	1,962
	TKN (w/o tp)	0.958	30.89	63	30	133	2,179	1,521
	TKN-Sequential	0.946	29.56	75	35	114	2,653	1,763
	TKN	0.958	30.89	64	11	364	2,561	1,587

Table 1. The results on KTH and Human3.6. \uparrow means the higher the better and \downarrow means the less the better. We skipped some tests due to the lack of original code. Instead, we used the results provided by the original papers (indicated by “*”), or skipped if the papers didn’t provide results (indicated by “-”). “w/o tp” means without temporal parallel and “seq” means sequential. We used 32 and 16 as the default batch sizes for KTH and Human3.6, but 16 and 8 for a few exceptions which otherwise exceeded the GPU capacity due to too many intermediate results generated by the algorithms. (30) indicates using 10 input frames to predict 30 frames with SLAMP. **Struct-VRNN** and **Grid-Keypoint** are Keypoint-based baselines.

Eq. (3) and then froze its parameters, then we trained the predictor using L_{pred} in (19). We found that this method trained faster than the end-to-end training which trained the keypoint detector and predictor together using both L_{rec} and L_{pred} .

Model structures. TKN and TKN-Sequential have the same keypoint detector structure, which has a 6-layer encoder and a 6-layer decoder. Each encoder layer includes Conv2D, GroupNorm, and LeakyRelu. Each decoder layer includes TransposedConv2D, GroupNorm and LeakyRelu. Since the skip connection is used between encoder and decoder, the input dimension of each decoder layer is twice the output dimension of the corresponding encoder layer.

For the predictor, TKN uses a 6-layer transformer encoder with the input sequence length of 10, and TKN-Sequential uses 10 single-layer transformer encoders, each with an input sequence length of 10, 11, ..., 19. As mentioned in Section Prediction Processes, each transformer encoder’s output of TKN-Sequential is averaged according to the input length, hence the output of both TKN and TKN-Sequential has a length of 10. All transformer encoders employed by the baselines share the same parameters: $d_k = d_v = 64$, $d_{model} = 512$, $d_{inner} = 2048$, $n_{head} = 8$, $dropout = 0$

Evaluation metrics. Traditional evaluation metrics include structural similarity (SSIM) and peak signal to noise ratio (PSNR). Higher SSIM indicates a higher similarity between the predicted image and the real image. Higher PSNR indicates better quality of the reconstructed image. We also quantify the resource (time and memory) consumption, for which a uniform batch size of 32 and 1

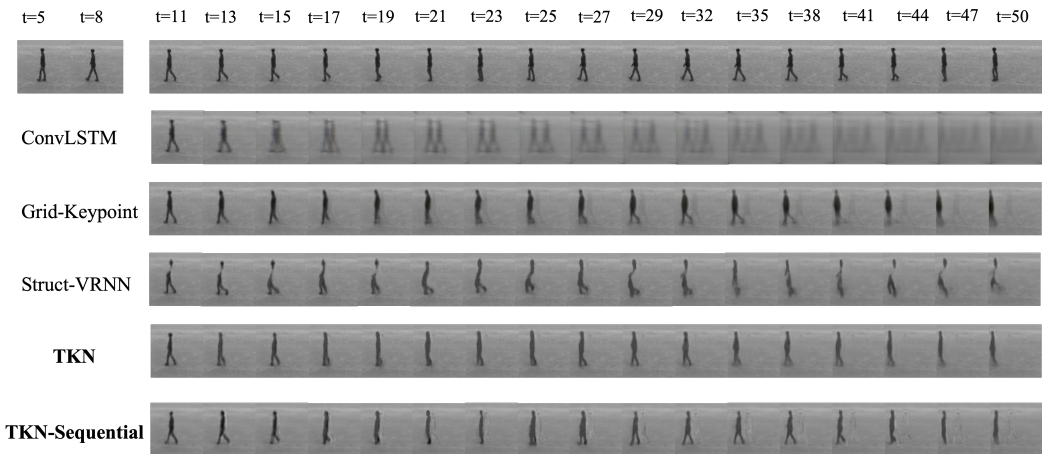


Fig. 7. Results of long-range predictions on KTH. TKN and TKN-Sequential perform better than the baselines. TKN-Sequential provides more precise details.

are used for KTH dataset during training and testing, and 16 and 1 are used for Human3.6 dataset during training and testing.

In addition, we measure the FLOPs (floating-point operations per second) to assess the computational cost and the number of parameters of the model with the thop¹ package.

Baselines. To validate the performance of TKN, we select 8 most classical and effective SOTA methods as the baselines, all of which are implemented with Pytorch for fair comparisons. The 8 baselines include: ConvLSTM[26], Struct-VRNN[21], Grid-Keypoint [10], Predrnn[32], Predennv2[33], PhyDNet[11], E3D-LSTM[31], SLAMP[1].

- (1) ConvLSTM[26] is one of the oldest and most classic video prediction method based on LSTM.
- (2) Struct-VRNN[21] is the first one to use keypoints to make prediction.
- (3) Grid-Keypoint[10] is a grid-based keypoint video prediction method.
- (4) Predrnn[32] is a classic prediction method adapted from LSTM.
- (5) Predennv2[33] can be generalized to most predictive learning scenarios by improving Predrnn with a new curriculum learning strategy.
- (6) PhyDNet[11] disentangles the dynamic objects and the static background in the video frames.
- (7) E3D-LSTM[31] combines 3DCNN and LSTM to improve prediction performance.
- (8) SLAMP[1] is an advanced stochastic video prediction method.
- (9) To highlight the importance of parallel prediction in terms of the fast prediction of TKN, particularly when compared with sequential keypoints method Struct-VRNN and Grid-Keypoint, we tested *TKN(w/o tp)* which has the same structure as TKN but lacks the parallel scheme of the keypoint detector.

Due to the lack or incompleteness of open-sourced code, we tested Predennv2 and SLAMP only on KTH dataset while the others on both datasets.

Method	boxing	handclapping	handwaving
TKN	0.897	0.908	0.898
TKN-Sequential	0.878	0.874	0.857
Method	jogging	running	walking
TKN	0.762	0.759	0.806
TKN-Sequential	0.783	0.775	0.820

Table 2. SSIM performances on different KTH's actions.

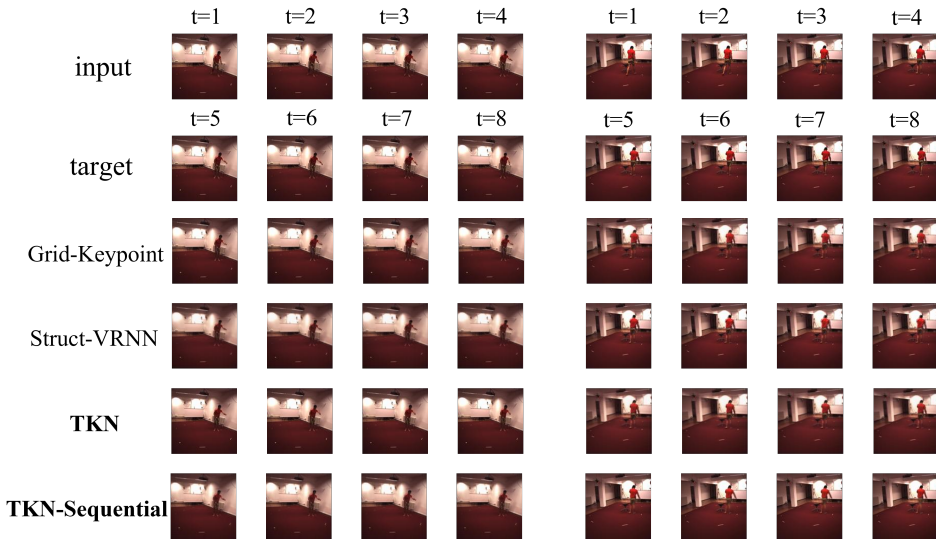


Fig. 8. Results of short-range predictions on Human3.6.

Method	MSE ↓	MAE ↓	SSIM ↑
ConvLSTM	103.3	182.9	0.707
PredRNN	56.8	126.1	0.867
PredRNNv2	48.4	-	0.891
PhyDNet	24.4	70.3	0.947
MIM	44.2	101.1	0.910
E3D-LSTM	41.3	86.4	0.910
CrevNet + ConvLSTM	38.5	-	0.928
CrevNet + ST-LSTM	22.3	-	0.949
SimVP	23.8	-	0.948
TKN	24.1	70.1	0.949
TKN-Sequential	24.7	72.9	0.945

Table 3. Quantitative Results on the Moving Mnist Dataset.

Method	SSIM \uparrow	PSNR \uparrow
BeyondMSE	0.847	-
MCnet	0.879	-
PredNet	0.905	27.6
ContextVP	0.921	28.7
rCycleGan	0.919	29.21
CrevNet	0.925	29.3
STMFANet	0.927	29.1
SimVP	0.940	33.1
TKN	0.925	29.6
TKN-Sequential	0.927	29.7

Table 4. Quantitative Results on the Caltech Pedestrian Dataset.

Method	Keypoint detector			Predictor		
	Time (ms)	FLOPs (G)	Params (M)	Time (ms)	FLOPs (G)	Params (M)
Struct-VRNN	104	11.8	0.8	38	0.1	3.5
Grid-Keypoint	142	17.7	1.8	84	8.5	1.7
TKN (w/o tp)	67	1.4	0.1	8.3	0.2	18.9
TKN	8.2	1.4	0.1	8.3	0.2	18.9

Table 5. Time, FLOPs, and the number of parameters comparisons between the Keypoint-based models.

5 RESULTS AND ANALYSIS

5.1 Speed and Accuracy

Table 1 summarizes the performance comparison on KTH and Human3.6 datasets. For KTH, we input 10 frames to predict 10 frames during training and 20 frames during testing. For Human3.6, we input 4 frames to predict 4 frames during both training and testing. *TIME (train)* refers to the average period length per training epoch in seconds. *Time (test)* indicates the period length from inputting the frames to after generating the predicted frames in milliseconds. *FPS* is the number of generated frames per second calculated via *Time (test)*. *Memory* indicates the maximum memory consumption at a stable status. Note that to ensure fair comparisons with the end-to-end training methods, *TIME (train)* and *Memory (train)* of TKN, Struct-VRNN and Grid-Keypoint in Table 1 are all tested without freezing parameters. The results show that TKN outperforms most baselines in both speed and memory consumption significantly with only minor accuracy deterioration on both datasets.

KTH results show that TKN performed 19 times faster than the best method E3D-LSTM with only 0.9% and 5.5% degradation in SSIM and PSNR during testing, while reducing memory consumption by at least 12.7% (training) and 0.9% (testing) compared to the second best methods Struct-VRNN and PredRNN. As such, TKN can bear up to as large a batch size as 150 with up to 24 GB memory which no baseline can even come close to. TKN is 4 times faster than TKN (w/o tp). Fig. 7 shows the performance of long-range prediction performance tested on the walking class of KTH, with 10 frames as input for predicting 40 frames. The result shows that the TKN predicts the position and pose of a person fairly well while TKN-Sequential presents more and clearer details, because

¹<https://pyip.org/project/thop/>

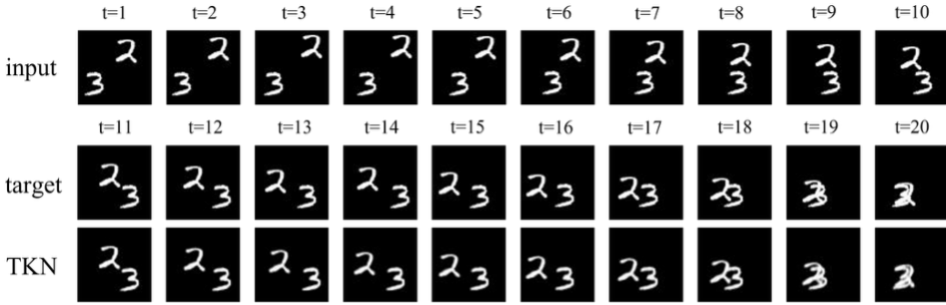


Fig. 9. Qualitative results on the Moving Mnist dataset. (10→10).

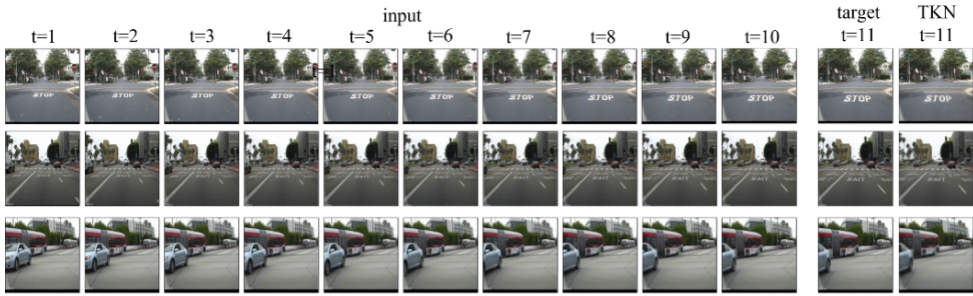


Fig. 10. Qualitative results on the Caltech Pedestrian dataset. (10→1).

TKN only uses the background information of a fixed frame to synthesize the following frames. We compare the performance of our models on the different action classes contained in KTH, each class with 100 randomly selected video sequences of each KTH’s action class for tests. As summarized in Table 2, TKN-Sequential performs better than TKN on actions with large movements such as walking, jogging, and running, while TKN performs better on handwaving, handclapping, and boxing which have smaller movements.

Human3.6 results show that TKN outperforms the baselines on accuracy performance. Moreover, TKN reduces time and memory consumption by 6% and 49% during training, and 66% and 9% during testing, compared to the second best alternative. Figure 8 depict the comparison of TKN and baselines on the Human3.6 dataset for short-range prediction, as most baselines do. The changes of the actions are small within a short period. But upon closer observation, we can tell that the lighting of the background and the movement of the person in TKN are closest to the goundtruth.

Moving Mnist and Caltech Pedestrian. We did not test the prediction speed on these two datasets since it’s only related to the image shape. As shown in Fig.9 and Fig.??, TKN predicted the outcomes with good accuracy on both Moving Mnist and Caltech Pedestrian datasets. As summarized in Tab.3 and Tab.4, TKN achieved comparable performances to the state-of-the-art (SOTA).

Deeper speed analysis. To help understand why TKN runs so much faster than SOTA algorithms, we measure FLOPs and the number of parameters for each method. TKN and TKN(w/o tp) share the same structure and thus have the same numbers of FLOPs and parameters. As shown in

Method	FLOPs (G) ↓	Params (M) ↓
ConvLSTM	93.7	4.8
PredRNN	29.4	6.0
PredRNNv2	29.6	6.1
PhyDNet	21.7	3.0
SLAMP	95.0	49.4
E3D-LSTM	270.2	3.7
GridNet	26.2	3.3
Struct-VRNN	11.8	4.3
TKN	1.6	19.1
TKN (w/o tp)	1.6	19.1
TKN-Sequential	3.5	105

Table 6. The results of FLOPs and the number of parameters. ↓ means the less the better.

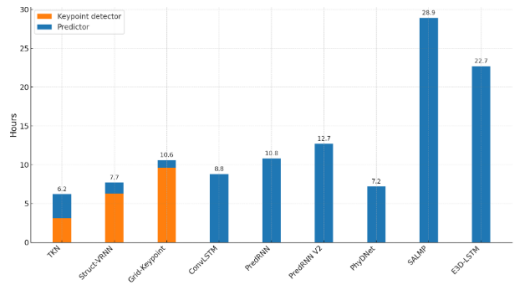


Fig. 11. Total training time of TKN and baselines.

Conv Kernel	SSIM	PSNR	Speed(ms)	FLOPs(G)	Params(M)
3×3	0.916	31.91	8.2	1.4	0.14
2×2	0.862	28.55	7.6	0.5	0.06
1×1	0.851	28.07	7.1	0.2	0.02
$3 \times 3, 1 \times 1$	0.900	30.84	7.8	0.9	0.08

Table 7. The influence of convolution kernel size on the reconstruction accuracy and inference speed of keypoint detector. “ $3 \times 3, 1 \times 1$ ” indicates using 1×1 convolution kernel for layers that change only the channel size and not the heatmap size and 3×3 convolution kernel for the other layers.



Fig. 12. Comparison of the keypoints extracted by different methods

Method	Num	Reconstruction		Prediction	
		SSIM	PSNR	SSIM	PSNR
Struct-VRNN	12	0.821*	27.86*	0.766*	24.29*
Grid-Keypoint	12	0.862*	29.68*	0.837*	27.11*
Separation-Net	16	0.900	30.95	0.855	26.81
TKN	4	0.895	30.43	0.850	26.66
	8	0.909	31.28	0.854	26.72
	12	0.914	31.71	0.863	27.40
	16	0.916	31.91	0.871	27.71
	20	0.915	31.95	0.861	27.23
	32	0.922	32.48	0.858	26.92
	64	0.925	32.71	0.849	26.46

Table 8. The results of frame reconstruction and prediction using different numbers of keypoints. “Separation-Net” refers to the structure in Figure 3(b). 12, 12, 16, are the number of keypoints when Struct-VRNN, Grid-Keypoint, and Separation-Net achieved their best performances, respectively.

Method	SSIM	PSNR	TIME (s)		FPS	Memory (MB)		FLOPs(G)	Params(M)
			train	test		train	test		
TKN	0.871	27.71	13	17	1,176	4,945	1,705	1.6	19.1
TKN+RNN	0.826	25.61	13	15	1,333	5,479	2,131	1.9	47.5
TKN+LSTM	0.815	25.19	19	23	870	9,343	4,287	3.3	189.1
TKN+GRU	0.829	25.82	17	22	1,000	8,029	3,567	2.8	141.9
TKN+MLP	0.814	25.12	13	13	1,538	4,841	1,733	1.5	14.4

Table 9. Performance comparison between TKN employing different predictors.

Method	SSIM	PSNR	TIME (ms)		FPS	Memory (MB)	TIMES (ms)
			all model(test)	Predictor(test)			
TKN (employs only the encoder)	0.871	27.71	17	1,176	1,705	8.3	
TKN (employs whole transformer)	0.800	25.87	93	215	1,759	74	

Table 10. Performance comparison of TKN’s prediction module between using only the transformer encoder and whole transformer.

Table 6, TKN and TKN-Sequential have much fewer FLOPs than the baselines, indicating their much higher computation efficiencies. Table 5 summarizes the detailed comparison between TKN, TKN(w/o tp), and the other two Keypoint-based methods. For the choice of predictor, TKN uses transformer encoder while Grid-Keypoint uses convlstm and Struct-VRNN uses VRNN. The results in Table 5 show that TKN presents the fastest speed in both modules and provides an 8 times speedup compared with TKN(w/o tp), indicating the key role of keypoint detector in terms of prediction speed and the advantage of parallel scheme. We can also find that although the predictor of TKN has more FLOPs and number of parameters due to the larger number of parameters of the employed transformer encoder [29], it runs about 5 to 10 times faster than the others.

Overall training time. We compare the overall training time considering various numbers of required epochs before convergence. Note that here TKN, Grid-Keypoint, and Struct-VRNN use the two-step training as mentioned in Section 4. Although TKN’s predictor trains slower than Grid-Keypoint and Struct-VRNN because its Transformer encoder takes 750 epochs to reach the

Method	SSIM	PSNR	Speed (ms)	FLOPs(G)	Params(M)
explicit	0.852	26.50	6.7	0.01	0.7
latent	0.871	27.71	8.3	0.19	18.9

Table 11. Comparison between using explicit and latent representation of keypoints.

optima while ConvLstm and VRNN takes only 20 and 50, TKN’s overall training speed is up to 2 to 3 times faster than the baselines as shown in Figure 11.

5.2 Ablation Experiments

Keypoint Detector. We test the impact of convolution kernel size and find that it presents a much larger impact on reconstruction accuracy than on inference speed of keypoint detector as summarized in Table 7. Therefore we choose to use the 3×3 convolution kernel.

Table 8 shows that TKN reconstructs frames better than the two Keypoints-based baselines and the sequential structure in Fig. 3(b), and achieves better performance with more keypoints. Meanwhile, the prediction module hits a performance bottleneck at 20 keypoints, indicating that too many keypoints pose difficulties for prediction. Figure 12 shows that the keypoint detector of TKN performs better at capturing dynamic information than that of Struct-VRNN and Grid-keypoint on different actions.

Predictor relies on the results of the keypoint detector. We verified its performance by replacing its Transformer encoder with alternative modules, i.e., RNN [9], LSTM [12], GRU [6], and MLP, which are widely used in prediction tasks. We adjusted the input dimension to $\mathbb{R}^{d_{model}}$ (512), number of layers to 6, and the dimension of the hidden layers to 2048, in all modules, for fair comparisons. We use the encapsulated RNN, LSTM, and GRU modules from PyTorch and use the MLP structure in Mlp-mixer[28]). As shown in Table 9, our predictor module presents comparable training and testing speeds with significantly higher accuracy and memory efficiency.

Table 10 compares the performance of TKN’s predictor employing the complete transformer structure with when using only its encoder part. We can see that the encoder-only method works much better in terms of both prediction speed and accuracy. This is because the transformer initially proposed for NLP problems requires embedding each word’s label ID into a vector. Its translation process is similar to RNN’s cycle principle which compares each high-dimensional output with the embedding vectors to get the word ID, and then inputs the corresponding embedding vector to the transformer to translate the next word. In short, their input and output are finite discrete quantities, while the keypoints in our prediction task are continuous quantities which cannot be labeled with finite IDs, hence excluding the possibility of mapping the high-dimensional output to IDs. Moreover, each output in our task, which is the next input, is a floating point which cannot be acquired with 100% accuracy. Thus, the small errors in each transformer cycle are accumulated. TKN employing the complete transformer has a long prediction time because the translation part of the transformer is a step-by-step process and each step goes through a complete transformer, while encoder-only TKN outputs all the results in one step.

Further, we test the impact of using explicit or latent representation of keypoints. As shown in Table 11, latent representation in high-dimension presents higher prediction accuracy. On the other hand, explicit representation only has limited speed improvement albeit it has fewer FLOPs and parameters.

6 CONCLUSION

This paper has presented TKN, a video prediction model that combines the advantages of keypoints and transformer models to achieve comparable accuracy performance with SOTA but with significantly less time and memory cost. TKN realizes real-time video prediction for the first time and opens the door for numerous futuristic applications demanding such capabilities. For future work, we plan to combine TKN with new AR applications and apply it to multi-person videos with higher resolutions.

REFERENCES

- [1] Adil Kaan Akan, Erkut Erdem, Aykut Erdem, and Fatma Güney. 2021. SLAMP: Stochastic Latent Appearance and Motion Prediction. In *Proceedings of the IEEE/CVF International Conference on Computer Vision*. 14728–14737.
- [2] Anurag Arnab, Mostafa Dehghani, Georg Heigold, Chen Sun, Mario Lučić, and Cordelia Schmid. 2021. Vivit: A video vision transformer. In *Proceedings of the IEEE/CVF International Conference on Computer Vision*. 6836–6846.
- [3] Andreas Blattmann, Timo Milbich, Michael Dorkenwald, and Bjorn Ommer. 2021. Understanding object dynamics for interactive image-to-video synthesis. In *Proceedings of the IEEE/CVF Conference on Computer Vision and Pattern Recognition*. 5171–5181.
- [4] Lluís Castrejon, Nicolas Ballas, and Aaron Courville. 2019. Improved conditional vrns for video prediction. In *Proceedings of the IEEE/CVF International Conference on Computer Vision*. 7608–7617.
- [5] Xinyuan Chen, Chang Xu, Xiaokang Yang, and Dacheng Tao. 2020. Long-term video prediction via criticism and retrospection. *IEEE Transactions on Image Processing* 29 (2020), 7090–7103.
- [6] Kyunghyun Cho, Bart Van Merriënboer, Caglar Gulcehre, Dzmitry Bahdanau, Fethi Bougares, Holger Schwenk, and Yoshua Bengio. 2014. Learning phrase representations using RNN encoder-decoder for statistical machine translation. *arXiv preprint arXiv:1406.1078* (2014).
- [7] Emily L Denton et al. 2017. Unsupervised learning of disentangled representations from video. *Advances in neural information processing systems* 30 (2017).
- [8] Alexey Dosovitskiy, Lucas Beyer, Alexander Kolesnikov, Dirk Weissenborn, Xiaohua Zhai, Thomas Unterthiner, Mostafa Dehghani, Matthias Minderer, Georg Heigold, Sylvain Gelly, et al. 2020. An image is worth 16x16 words: Transformers for image recognition at scale. *arXiv preprint arXiv:2010.11929* (2020).
- [9] Jeffrey L Elman. 1990. Finding structure in time. *Cognitive science* 14, 2 (1990), 179–211.
- [10] Xiaojie Gao, Yueming Jin, Qi Dou, Chi-Wing Fu, and Pheng-Ann Heng. 2021. Accurate Grid Keypoint Learning for Efficient Video Prediction. In *2021 IEEE/RSJ International Conference on Intelligent Robots and Systems (IROS)*. IEEE, 5908–5915.
- [11] Vincent Le Guen and Nicolas Thome. 2020. Disentangling physical dynamics from unknown factors for unsupervised video prediction. In *Proceedings of the IEEE/CVF Conference on Computer Vision and Pattern Recognition*. 11474–11484.
- [12] Sepp Hochreiter and Jürgen Schmidhuber. 1997. Long short-term memory. *Neural computation* 9, 8 (1997), 1735–1780.
- [13] Catalin Ionescu, Dragos Papava, Vlad Olaru, and Cristian Sminchisescu. 2014. Human3.6M: Large Scale Datasets and Predictive Methods for 3D Human Sensing in Natural Environments. *IEEE Transactions on Pattern Analysis and Machine Intelligence* 36, 7 (jul 2014), 1325–1339.
- [14] Tomas Jakab, Ankush Gupta, Hakan Bilen, and Andrea Vedaldi. 2018. Conditional image generation for learning the structure of visual objects. *methods* 43 (2018), 44.
- [15] Jingyun Liang, Jiezhang Cao, Guolei Sun, Kai Zhang, Luc Van Gool, and Radu Timofte. 2021. Swinir: Image restoration using swin transformer. In *Proceedings of the IEEE/CVF International Conference on Computer Vision*. 1833–1844.
- [16] Ze Liu, Yutong Lin, Yue Cao, Han Hu, Yixuan Wei, Zheng Zhang, Stephen Lin, and Baining Guo. 2021. Swin transformer: Hierarchical vision transformer using shifted windows. In *Proceedings of the IEEE/CVF International Conference on Computer Vision*. 10012–10022.
- [17] Ze Liu, Jia Ning, Yue Cao, Yixuan Wei, Zheng Zhang, Stephen Lin, and Han Hu. 2021. Video swin transformer. *arXiv preprint arXiv:2106.13230* (2021).
- [18] Ze Liu, Jia Ning, Yue Cao, Yixuan Wei, Zheng Zhang, Stephen Lin, and Han Hu. 2022. Video swin transformer. In *Proceedings of the IEEE/CVF Conference on Computer Vision and Pattern Recognition*. 3202–3211.
- [19] Daniel V McGehee, Elizabeth N Mazzae, and GH Scott Baldwin. 2000. Driver reaction time in crash avoidance research: Validation of a driving simulator study on a test track. In *Proceedings of the human factors and ergonomics society annual meeting*, Vol. 44. Sage Publications Sage CA: Los Angeles, CA, 3–320.
- [20] Min Meng and Jun Yu. 2018. Zero-shot learning via robust latent representation and manifold regularization. *IEEE Transactions on Image Processing* 28, 4 (2018), 1824–1836.

- [21] Matthias Minderer, Chen Sun, Ruben Villegas, Forrester Cole, Kevin P Murphy, and Honglak Lee. 2019. Unsupervised learning of object structure and dynamics from videos. *Advances in Neural Information Processing Systems* 32 (2019).
- [22] Marc Oliu, Javier Selva, and Sergio Escalera. 2018. Folded recurrent neural networks for future video prediction. In *Proceedings of the European Conference on Computer Vision (ECCV)*. 716–731.
- [23] Antti Rasmus, Mathias Berglund, Mikko Honkala, Harri Valpola, and Tapani Raiko. 2015. Semi-supervised learning with ladder networks. *Advances in neural information processing systems* 28 (2015).
- [24] Olaf Ronneberger, Philipp Fischer, and Thomas Brox. 2015. U-net: Convolutional networks for biomedical image segmentation. In *International Conference on Medical image computing and computer-assisted intervention*. Springer, 234–241.
- [25] Christian Schudt, Ivan Laptev, and Barbara Caputo. 2004. Recognizing human actions: a local SVM approach. In *Proceedings of the 17th International Conference on Pattern Recognition, 2004. ICPR 2004.*, Vol. 3. IEEE, 32–36.
- [26] Xingjian Shi, Zhourong Chen, Hao Wang, Dit-Yan Yeung, Wai-Kin Wong, and Wang-chun Woo. 2015. Convolutional LSTM network: A machine learning approach for precipitation nowcasting. *Advances in neural information processing systems* 28 (2015).
- [27] Hong Tao, Chenping Hou, Yuhua Qian, Jubo Zhu, and Dongyun Yi. 2020. Latent complete row space recovery for multi-view subspace clustering. *IEEE Transactions on Image Processing* 29 (2020), 8083–8096.
- [28] Ilya O Tolstikhin, Neil Houlsby, Alexander Kolesnikov, Lucas Beyer, Xiaohua Zhai, Thomas Unterthiner, Jessica Yung, Andreas Steiner, Daniel Keysers, Jakob Uszkoreit, et al. 2021. Mlp-mixer: An all-mlp architecture for vision. *Advances in Neural Information Processing Systems* 34 (2021), 24261–24272.
- [29] Ashish Vaswani, Noam Shazeer, Niki Parmar, Jakob Uszkoreit, Llion Jones, Aidan N Gomez, Łukasz Kaiser, and Illia Polosukhin. 2017. Attention is all you need. *Advances in neural information processing systems* 30 (2017).
- [30] Yunbo Wang, Zhifeng Gao, Mingsheng Long, Jianmin Wang, and S Yu Philip. 2018. Predrnn++: Towards a resolution of the deep-in-time dilemma in spatiotemporal predictive learning. In *International Conference on Machine Learning*. PMLR, 5123–5132.
- [31] Yunbo Wang, Lu Jiang, Ming-Hsuan Yang, Li-Jia Li, Mingsheng Long, and Li Fei-Fei. 2018. Eidetic 3d lstm: A model for video prediction and beyond. In *International conference on learning representations*.
- [32] Yunbo Wang, Mingsheng Long, Jianmin Wang, Zhifeng Gao, and Philip S Yu. 2017. Predrnn: Recurrent neural networks for predictive learning using spatiotemporal lstms. *Advances in neural information processing systems* 30 (2017).
- [33] Yunbo Wang, Haixu Wu, Jianjin Zhang, Zhifeng Gao, Jianmin Wang, S Yu Philip, and Mingsheng Long. 2022. Predrnn: A recurrent neural network for spatiotemporal predictive learning. *IEEE Transactions on Pattern Analysis and Machine Intelligence* 45, 2 (2022), 2208–2225.
- [34] Yunbo Wang, Haixu Wu, Jianjin Zhang, Zhifeng Gao, Jianmin Wang, Philip S Yu, and Mingsheng Long. 2021. PredRNN: A recurrent neural network for spatiotemporal predictive learning. *arXiv preprint arXiv:2103.09504* (2021).
- [35] Zhenjia Xu, Zhijian Liu, Chen Sun, Kevin Murphy, William T Freeman, Joshua B Tenenbaum, and Jiajun Wu. 2019. Unsupervised discovery of parts, structure, and dynamics. *arXiv preprint arXiv:1903.05136* (2019).
- [36] Guohao Ying, Yingtian Zou, Lin Wan, Yiming Hu, and Jiashi Feng. 2018. Better guider predicts future better: Difference guided generative adversarial networks. In *Asian Conference on Computer Vision*. Springer, 277–292.
- [37] Jingyu Zhao, Feiqing Huang, Jia Lv, Yanjie Duan, Zhen Qin, Guodong Li, and Guangjian Tian. 2020. Do rnn and lstm have long memory?. In *International Conference on Machine Learning*. PMLR, 11365–11375.
- [38] Tongxue Zhou, Stéphane Canu, Pierre Vera, and Su Ruan. 2021. Latent correlation representation learning for brain tumor segmentation with missing MRI modalities. *IEEE Transactions on Image Processing* 30 (2021), 4263–4274.

Received 20 February 2007; revised 12 March 2009; accepted 5 June 2009